

Fusion measurements for the $^{18}\text{O}+^{194}\text{Pt}$ reaction and search for neutron shell closure effects

This content has been downloaded from IOPscience. Please scroll down to see the full text.

2015 J. Phys. G: Nucl. Part. Phys. 42 095105

(<http://iopscience.iop.org/0954-3899/42/9/095105>)

View [the table of contents for this issue](#), or go to the [journal homepage](#) for more

Download details:

IP Address: 133.1.86.32

This content was downloaded on 04/01/2016 at 10:21

Please note that [terms and conditions apply](#).

Fusion measurements for the $^{18}\text{O}+^{194}\text{Pt}$ reaction and search for neutron shell closure effects

P V Laveen¹, E Prasad^{1,11}, N Madhavan², S Pal^{3,12},
J Sadhukhan⁴, S Nath², J Gehlot², A Jhingan², K M Varier⁵,
R G Thomas⁶, A M Vinodkumar⁷, A Shamlath¹, T Varughese²,
P Sugathan², B R S Babu⁸, S Appannababu², K S Golda²,
B R Behera⁹, Varinderjit Singh^{9,13}, Rohit Sandal^{9,14},
A Saxena⁶, B V John⁶ and S Kailas^{6,10}

¹ Department of Physics, School of Mathematical and Physical Sciences, Central University of Kerala, Kasaragod 671314, India

² Inter University Accelerator Centre, Aruna Asaf Ali Marg, New Delhi 110067, India

³ CS-6/1, Golf Green, Kolkata 700095, India

⁴ Physics Group, Variable Energy Cyclotron Centre, 1/AF Bidhan Nagar, Kolkata 700064, India

⁵ Department of Physics, University College, Trivandrum, Kerala, India

⁶ Nuclear Physics Division, Bhabha Atomic Research Centre, Mumbai 400085, India

⁷ Department of Physics, University of Calicut, Calicut 673635, India

⁸ Department of Physics, Sultan Qaboos University, Muscat, Oman

⁹ Department of Physics, Panjab University, Chandigarh 160014, India

¹⁰ UM-DAE Centre for Excellence in Basic Sciences, University of Mumbai, Mumbai 400098, India

¹¹ Department of Nuclear Physics, Research School of Physical Sciences and Engineering, The Australian National University, Canberra, ACT 2601, Australia

¹² Formerly with Variable Energy Cyclotron Centre, Kolkata, India

¹³ Department of Chemistry and Center for Exploration of Energy and Matter, Indiana University 2401 Milo B. Sampson Lane, Bloomington, Indiana 47408, USA

¹⁴ S V Govt. College Ghumarwin, Bilaspur 174021 (HP), India

E-mail: prasad.e.nair@gmail.com

Received 5 May 2015, revised 23 June 2015

Accepted for publication 30 June 2015

Published 27 July 2015



CrossMark

Abstract

Evaporation residue (ER) and fission cross sections were measured for the reaction $^{18}\text{O}+^{194}\text{Pt}$ forming the compound nucleus ^{212}Rn . Fission fragment angular distributions and anisotropies are consistent with the saddle point model predictions. Measured ER cross sections were fitted with statistical model calculations assuming shell-corrected free energy fission barrier height.

The non-zero dissipation strength required to fit the ER cross section supports the dissipative nature of fission dynamics in heavy ion fusion. In the present study shell closure effects are not observed in the dissipation strength.

Keywords: compound nucleus, fusion–fission, statistical model, nuclear dissipation, fission hindrance, evaporation residue

(Some figures may appear in colour only in the online journal)

1. Introduction

Heavy ion fusion reactions are particularly important as the most successful mechanisms for the production of superheavy elements (SHE) [1–4]. The SHE are expected to provide a very different testing ground for our present understanding about the complex and enigmatic nuclear matter. The existence of such extreme nuclear landscape is primarily facilitated by the stabilizing effects of shell structure. The formation of such heavy elements depends on the capture probability of the projectile-target systems inside the interaction barrier followed by the probability of ending up in a completely equilibrated compound nucleus (CN) and finally the survival probability of this heavy nucleus against fission. The heavy residual nucleus that survives the fission is the evaporation residue (ER) and is the true signature for the formation of the CN. The crossing of barrier and subsequent capture inside the potential barrier at near Coulomb barrier region are enhanced by the coupling to various internal degrees of freedom [5–7]. However, experimental results from reactions using projectiles heavier than oxygen unambiguously demonstrated that overcoming the interaction barrier will not necessarily ensure the formation of the CN. The capture flux will be shared among various non-compound nuclear (NCN) processes in addition to complete fusion. These NCN processes include quasifission [8–10], fast fission [11, 12] and pre-equilibrium fission [13]. The onset of these NCN processes may be inferred from the precise ER measurements [14, 15], fission fragment angular distribution studies [8, 16, 17] and fission fragment mass distribution measurements [10, 18–20]. Since NCN processes severely hinder the formation of the CN, the relative strengths of these processes essentially decide the CN formation probability.

A principal factor that decides the survival probability of the CN against fission is the fission barrier height. Fission barrier consists of two components, a macroscopic component and a microscopic component. While the macroscopic component originates from the competition between the surface and Coulomb forces, the microscopic component finds its origin in the shell correction energies. The uncertainty in the estimation of fission barrier heights is a major issue in calculating the survival probability of the CN. An average discrepancy of 1 MeV [21] between the experimental data and theoretical predictions could lead to an order of magnitude difference in fission cross sections. Even though the shell correction term has appreciably large values for many systems populated with neutron number around the neutron magic number $N = 126$, no significant stabilizing effects of ER against fission have been reported in literature [22–24]. There are strong speculations that the shell closure at $Z = 82$ and $N = 126$ may favour the survival probability of the CN against fission. A positive experimental indication in this regard with $N = 126$ may have path breaking consequences in SHE production, as shell model predicts next neutron shell closure at $N = 184$.

Another important factor that enhances the ER survival probability against fission is the dynamical delay in fission. Dynamical processes lead to the dissipation of energy stored in collective degrees of freedom to the internal degrees of freedom. These effects are more

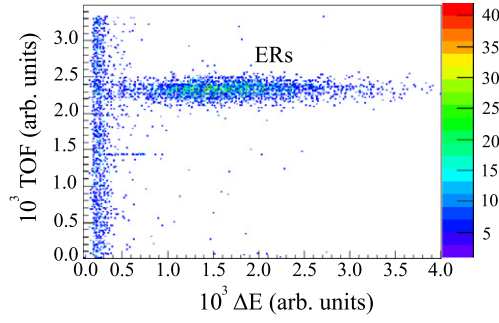


Figure 1. Two-dimensional spectrum of ΔE versus TOF at 100.2 MeV beam energy. The ERs are well separated from other contaminations.

relevant in heavy nuclei with $\frac{Z^2}{A} > 32$ [25], where Z is the atomic number and A is the mass number of the nucleus, respectively. The observation of enhanced pre-scission neutron multiplicities [25–28], charged particle multiplicities [29, 30] and GDR gammas [31–33] over the predictions of statistical model calculations indicated the necessity of a dynamical treatment including dissipation, to reproduce the experimental data. The dissipative mechanism also leads to an increased ER cross section [34–37] over the predictions of statistical model or dynamical model with zero viscosity. The most important advantage of ER in this context is their unique, complete sensitivity to pre-saddle dissipation.

In order to address some of these issues, we measured the ER and fission cross sections for the $^{18}\text{O}+^{194}\text{Pt}$ reaction forming the ^{212}Rn CN. The results are compared with a few other measurements available in the literature. ER measurements were performed using the recoil mass separator HYbrid Recoil Mass Analyzer (HYRA) [38] at Inter University Accelerator Centre (IUAC), New Delhi. The fission measurements were performed at the BARC-TIFR 14UD Pelletron accelerator facility at Mumbai.

2. Experimental details

The ER measurements were performed using the 15UD Pelletron accelerator facility at IUAC. Pulsed ^{18}O beam with $4\ \mu\text{s}$ pulse separation was used to bombard the isotopically enriched ^{194}Pt target of thickness $265\ \mu\text{g cm}^{-2}$ on $10\ \mu\text{g cm}^{-2}$ thick carbon backing (facing the beam). The heavy ERs produced in the reaction were separated from the intense beam background using the first stage of HYRA operated in gas-filled mode with helium gas at an optimized pressure of 0.15 Torr [36]. A $660\ \mu\text{g cm}^{-2}$ thick carbon foil was used as the pressure window foil, which separated the gas-filled region of HYRA from beam-line vacuum. The measurements were performed at laboratory beam energies (after correcting energy loss in pressure window foil, carbon backing and half-target thickness) of 77.7, 82.8, 86.9, 92.0, 96.1, 100.2 and 105.3 MeV. Two silicon detectors were used inside the target chamber, placed at $\theta = \pm 22.7^\circ$, to detect the elastically scattered particles and flux normalization. The Rutherford-scattered beam-like particles recorded in these detectors were used for ER cross section normalization. These detectors were also used for positioning the beam at the center of the target. The ERs reaching the focal plane were detected using a position sensitive multi-wire proportional counter (MWPC) of active area $15 \times 5\ \text{cm}^2$ [39]. This detector was operated with isobutane gas at 2 mbar pressure and it provided two-dimensional position (X, Y) signals, energy loss signal (cathode) and timing signal (anode). These position signals were processed

through the constant fraction discriminators and fed to the time to digital converter as stop signals, with anode signal as the common start.

A time of flight (TOF) signal was generated from the MWPC anode (start signal) and the delayed RF-pulse with $4 \mu\text{s}$ pulse separation (stop signal) which enabled an unambiguous separation of ERs from beam-like and target-like contaminations. Figure 1 shows the two-dimensional plot of this energy loss (ΔE) signal versus TOF signal at 100.2 MeV beam energy. The data were collected and analyzed using the IUAC data sorting software CANDLE [40].

The fission measurements were performed in a separate experiment using the scattering chamber of BARC-TIFR 14UD Pelletron accelerator facility. ^{18}O beam (dc) in the energy range 78.2–87.3 MeV was used to bombard ^{194}Pt target in this measurement. The fission fragments were collected using three ΔE – E silicon detector telescopes consisting of 15–20 μm thick ΔE detectors and 300–500 μm thick E detectors. An aluminium collimator of diameter 5 mm was used in front of each telescope assembly. These telescopes were placed at 13.6 cm from the target, on the same movable arm of the scattering chamber. Two silicon surface barrier detectors were mounted at $\theta = \pm 20^\circ$ with respect to the beam direction, at a distance of 42 cm from the target center. The elastic events recorded in these detectors were used for the normalization of the fission yields and estimation of the absolute differential cross sections. The angular distribution of the fission fragments were measured at 10° intervals from 80° to 170° in the laboratory frame. The trigger for the data acquisition system was derived from the ΔE detector signals. The relative solid angles of the telescopes were extracted by measuring the data at overlapping angles. Most of the fragments were stopped within the thin ΔE detectors and fragments reaching the E detectors were well separated in energy from elastic, quasi elastic and other possible channels.

3. Data analysis and results

3.1. ER cross section

The total ER cross section is given by

$$\sigma_{\text{ER}} = \frac{Y_{\text{ER}}}{Y_{\text{mon}}} \left(\frac{d\sigma}{d\Omega} \right)_{\text{R}} \Omega_M \frac{1}{\epsilon_{\text{HYRA}}}, \quad (1)$$

where σ_{ER} is the total ER cross section in mb, Y_{ER} is the number of ERs detected at the focal plane detector of HYRA, Y_{mon} is the number of elastically scattered beam particles detected in the monitor detector, $\left(\frac{d\sigma}{d\Omega} \right)_{\text{R}}$ is the differential Rutherford scattering cross section in the laboratory system, Ω_M is the solid angle subtended by the collimated monitor detector at target center and ϵ_{HYRA} is the HYRA transmission efficiency. In this run, we used $^{16}\text{O}+^{194}\text{Pt}$ reaction as the calibration reaction, for which ER cross sections are already reported [36]. The ER cross section for this calibration reaction was measured at 91.9 and 95.9 MeV (laboratory energies) and the transmission efficiency for this calibration reaction is calculated using equation (1). Since ϵ_{HYRA} depends on various factors [36, 41], its value is expected to be different for different reactions and also at different beam energies. ϵ_{HYRA} for $^{18}\text{O}+^{194}\text{Pt}$ reaction is thus estimated by comparing the normalized angular distributions of $^{18}\text{O}+^{194}\text{Pt}$ and $^{16}\text{O}+^{194}\text{Pt}$ (calibration reaction) using an exactly similar procedure detailed in our previous works [36, 42, 43]. The semi-microscopic Monte Carlo code TERS [44] is used for simulating the angular, energy and charge distributions of the ERs produced in these two reactions. The acceptance angle of the present setup is limited by the narrow aperture of the target chamber

Table 1. Measured ER cross section (σ_{ER}) at various center-of-mass energies.

$E_{c.m.}$ (MeV)	σ_{ER} (mb)
71.1	50 ± 10
75.8	214 ± 43
79.5	347 ± 69
84.2	387 ± 77
87.9	401 ± 63
91.7	366 ± 73
96.4	316 ± 63

used, translating to a polar angle of 3.4° [42]. The variation of the estimated ϵ_{HYRA} values is not very significant in the energy range studied in this work. The experimental total ER cross section as a function of center-of-mass energy is given in table 1. The overall errors are $\leq 20\%$, out of which ϵ_{HYRA} contributes the maximum uncertainty.

3.2. Fission cross sections

The measured fission fragment angular distributions are transformed from laboratory to center-of-mass frame using Viola systematics for symmetric fission [45]. Energy loss corrections of the beam in the half target thickness is applied before conversion to the center-of-mass frame. The differential fission cross section is calculated using the expression

$$W(\theta_{\text{cm}}) \propto \frac{d\sigma_{\text{fis}}}{d\Omega} = \frac{1}{2} \frac{Y_{\text{fis}}}{Y_{\text{mon}}} \left(\frac{d\sigma}{d\Omega} \right)_{\text{R}} \frac{\Omega_{\text{mon}}}{\Omega_{\text{fis}}} G, \quad (2)$$

where G is the Jacobian of laboratory frame to center-of-mass frame transformation. Y_{fis} and Y_{mon} are the yields recorded by the fission detector and monitor (Rutherford-scattering) detector, respectively. Ω_{fis} and Ω_{mon} are the solid angles subtended by the fission and monitor detectors, respectively. The total fission cross section σ_{fis} is then obtained by integrating the differential cross sections. The experimental fission fragment angular distributions are fitted using the standard expressions [17, 46]. Under these assumptions, the fission fragment angular distributions can be represented as

$$W(\theta) = \frac{\sum_{J=0}^{\infty} (2J+1) T_J \frac{\sum_{K=-J}^J \frac{1}{2} (2J+1) d_{0K}^J(\theta)^2 \exp\left[\frac{-K^2}{2K_0^2(J)}\right]}{\sum_{K=-J}^J \exp\left[\frac{-K^2}{2K_0^2(J)}\right]}, \quad (3)$$

where T_J is the transmission coefficient for fusion of the J th partial wave, $K_0^2 = \frac{I_{\text{eff}}}{\hbar^2} T$, is the variance of the K distribution and I_{eff} is the effective moment of inertia at the saddle point. The saddle point temperature (T) is calculated using the expression $T = \sqrt{E^*/a}$, where E^* is the excitation energy of the fissioning nucleus ($E^* = E_{c.m.} + Q - B_f(l) - E_{\text{rot}}(l) - E_n$) and ' a ' is the level density parameter. Here, $E_{c.m.} + Q$ is the excitation energy of the CN, $B_f(l)$ and $E_{\text{rot}}(l)$ are the angular momentum dependent fission barrier height and rotational energy, respectively. E_n is the reduction in the excitation energy of the system due to the evaporation of neutrons. In this analysis, we set $E_n = N_{\text{pre}} \times 10 \text{ MeV}$, where N_{pre} is the pre-scission neutron multiplicity. The I_{eff} , B_f and E_{rot} values are calculated using the rotating finite range model [47]. The experimental angular distributions and best fittings are shown in figure 2 at

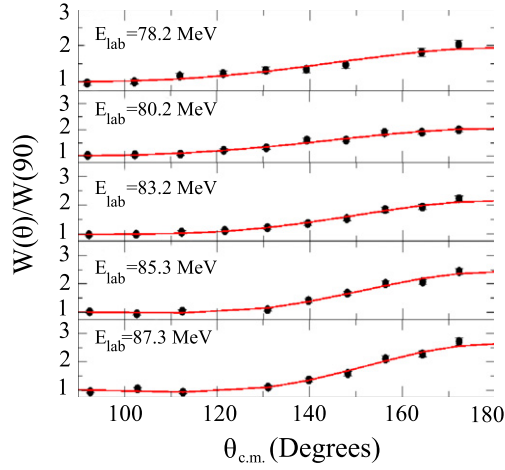


Figure 2. Fission fragment angular distributions at different laboratory energies. The red solid line is the fit to the experimental angular distribution.

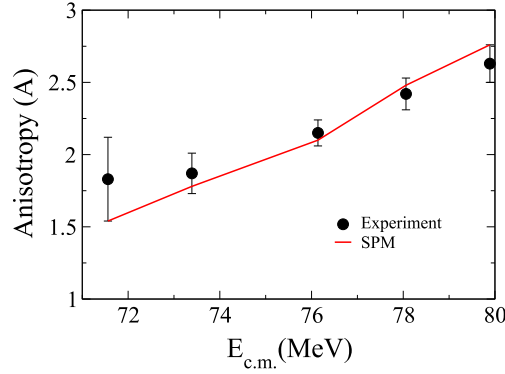


Figure 3. Experimental fission fragment angular anisotropy at different centre-of-mass energies. The red solid line is the SPM prediction.

different energies. Fission fragment angular anisotropies $\left(A = \frac{W(180^\circ)}{W(90^\circ)}\right)$ are hence obtained from the above fit.

Under the saddle point model (SPM) [17, 46], the fragment angular anisotropy is given by the simplified formula

$$A = 1 + \frac{\langle l^2 \rangle}{4K_0^2}, \quad (4)$$

where $\langle l^2 \rangle$ is the mean square angular momentum of the fissioning system.

The $\langle l^2 \rangle$ -values are calculated using the PACE code [48], using the CN spin distribution as the input which is obtained from the coupled channels code CCFULL [49, 50] by reproducing the experimental total fusion cross sections. The total fusion cross sections are obtained by summing the ER and fission cross sections. Since experimental ER and fission cross sections are not available at same excitation energies, interpolated values of fission cross sections at excitation energies where ER cross sections are measured are used to obtain the

Table 2. The saddle point temperature (T), mean square angular momentum ($\langle l^2 \rangle$), fission cross section (σ_{fis}) and angular anisotropy (A) at different energies are shown here.

$E_{c.m.}$ (MeV)	T (MeV)	$\langle l^2 \rangle \hbar^2$	σ_{fis} (mb)	A
71.6	0.97	170.3	12 ± 1	1.83 ± 0.29
73.4	0.98	253.6	30 ± 2	1.87 ± 0.14
76.1	1.01	371.2	69 ± 5	2.15 ± 0.09
78.0	1.02	503.5	104 ± 7	2.42 ± 0.11
79.9	1.03	601.6	153 ± 11	2.63 ± 0.13

Table 3. The CCFULL potential parameters used in calculations for obtaining CN spin distribution for different reactions.

Reaction	V_0 (MeV)	r_0 (fm)	a (fm)
$^{16}\text{O}+^{194}\text{Pt}$	64.38	1.19	0.6565
$^{18}\text{O}+^{194}\text{Pt}$	64.00	1.19	0.6606
$^{16}\text{O}+^{186}\text{Os}$	64.04	1.19	0.6558
$^{18}\text{O}+^{192}\text{Os}$	63.77	1.19	0.6604

total fusion cross sections. The rotational couplings of the target nucleus are included in the CCFULL calculations while reproducing the total fusion cross sections. The same spin distribution is also used as the input to the statistical model calculations performed to reproduce the ER cross section data, discussed in section 4. The N_{pre} values are either obtained from [51] for matching excitation energies or calculated using the systematics given in [25]. The experimental angular anisotropies compared with the SPM estimates are shown in figure 3. The uncertainties quoted in the anisotropy values are statistical in nature. The experimental fission cross section, angular anisotropy and different parameters used in the SPM calculations are given in table 2. The CCFULL potential parameters used for different reactions discussed in this article are given in table 3.

4. Statistical model analysis

In the present statistical model calculations of ER cross section, it is assumed that the composite system after capture forms the CN and, contributions from other NCN channels are negligible. This is experimentally verified by measuring the fission fragment angular distributions and angular anisotropies at near barrier energies. The angular distribution measurements for $^{18}\text{O}+^{194}\text{Pt}$ reaction are discussed in the previous section and those of $^{16}\text{O}+^{194}\text{Pt}$ system are reported in [52]. The highly excited CN decays via light particle emission (mainly neutrons, protons and α -particles), statistical γ -decay and fission. All these possibilities are taken into account in the present calculations. The particle evaporation and γ emission widths are obtained from the standard Weisskopf formula [53]. The level density parameter used to obtain various decay widths is taken from the work of Ignatyuk *et al* [54] where the effect of shell structure in reducing the level density at low excitation energies is included and is given as follows:

$$a(\mathbf{q}, U) = \tilde{a}(\mathbf{q}) \left[1 + \frac{f(U)}{U} \delta W \right], \quad (5)$$

$$f(U) = 1 - \exp(-U/E_D), \quad (6)$$

where U is the thermal energy of the CN, δW is the shell correction energy taken from the difference between the experimental and liquid drop model masses, E_D accounts for the rate at which the shell effect melts away with increase of excitation energy, and $\tilde{a}(\mathbf{q})$ is the asymptotic value to which the level density parameter approaches with increasing excitation energy of the CN. \tilde{a} depends upon the nuclear mass number and the shape, specified by the collective coordinates \mathbf{q} , in a fashion similar to the liquid drop model of mass and its values are taken from [55].

The calculations are performed using the fission width from the Kramers' formalism [56] where the fission dynamics is assumed to be similar to that of a Brownian particle in a heat bath. It has been pointed out earlier that the driving force in a thermodynamical system like a hot nucleus is provided by the free energy rather than the potential energy of the system [57, 58]. The free energy F is given in the Fermi gas model as

$$F(\mathbf{q}, T) = V(\mathbf{q}) - \tilde{a}(\mathbf{q}) T^2, \quad (7)$$

where T is the CN temperature and $V(\mathbf{q})$ is the zero-temperature potential energy. The finite-range liquid drop model potential (FRLDM) [47] is used for $V(\mathbf{q})$.

The fission width due to Kramers (Γ_K), which includes the effect of nuclear dissipation is given as [56, 58],

$$\Gamma_K = \frac{\hbar \omega_g(T)}{2\pi} \exp\left(\frac{-F_B}{T}\right) \left(\sqrt{1 + \left(\frac{\beta}{2\omega_s(T)}\right)^2} - \frac{\beta}{2\omega_s(T)} \right), \quad (8)$$

where β denotes the dissipation coefficient and $F_B(T)$ is the free energy fission barrier. In the above equation, $\omega_g(T)$ and $\omega_s(T)$ are the frequencies of the harmonic oscillators which have the same curvatures as that of the free energy profile at the ground state and at the saddle configuration of the CN, respectively. It may be pointed out here that for $\beta = 0$, equation (8) reduces to the following form of the Bohr–Wheeler fission width in free energy profile [58],

$$\Gamma_{BW}^F = \frac{\hbar \omega_g(T)}{2\pi} \exp\left(\frac{-F_B(T)}{T}\right). \quad (9)$$

We further include shell correction in the free energy fission barrier which is given as [59],

$$F_B^{\text{shell}}(T) = F_B^{\text{no-shell}}(T) - \delta W \exp\left(-\frac{U}{E_D}\right). \quad (10)$$

The Kramers' fission width of equation (8) represents a stationary fission rate which is reached after an initial delay or the transient time. This is taken into account in the statistical model calculation by using the following parametrized form of the time-dependent fission width [60],

$$\Gamma_f(t) = \Gamma_K \left[1 - \exp(-2.3t/\tau_f) \right], \quad (11)$$

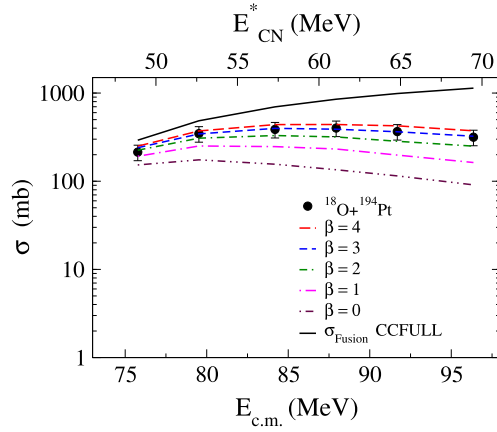


Figure 4. Experimental ER cross sections for the $^{18}\text{O}+^{194}\text{Pt}$ reaction compared with statistical model calculations using different values of β (in unit of 10^{21} s^{-1}). Total fusion cross section calculated using coupled channels code CCFULL is also shown. The CN excitation energy (E^*) is shown on the top of X -axis.

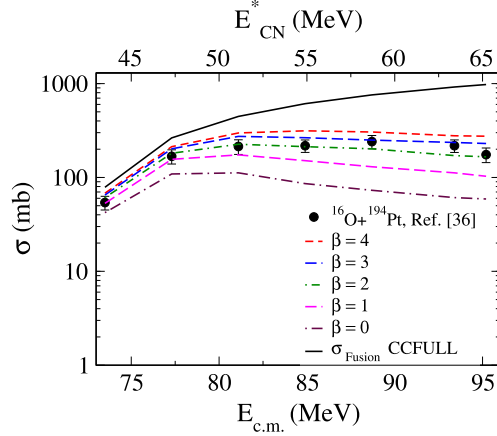


Figure 5. Experimental ER cross sections for $^{16}\text{O}+^{194}\text{Pt}$ reaction [36] compared with statistical model calculations using different values of β (in unit of 10^{21} s^{-1}). Total fusion cross section calculated using coupled channels code CCFULL is also shown. The CN excitation energy (E^*) is shown on the top of X -axis.

where the transient time τ_f is given as

$$\tau_f = \frac{\beta}{2\omega_g^2} \ln \left(\frac{10F_B}{T} \right). \quad (12)$$

The simulation of a CN decay in the statistical model is performed by following it in time over small time steps and, at each time step, the fate of the CN is decided by a Monte Carlo sampling using particle, γ and the fission widths [61]. The initial CN spin distribution for each initial excitation energy is obtained from CCFULL. The evaporation of particles and γ -rays changes the excitation energy and spin of the residual nucleus. The changes thus produced are

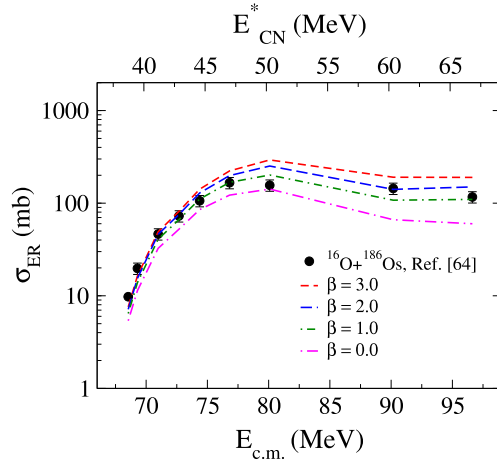


Figure 6. Experimental ER cross sections for $^{16}\text{O}+^{186}\text{Os}$ reaction [64] compared with statistical model calculations using different values of β (in unit of 10^{21} s^{-1}). Total fusion cross section calculated using coupled channels code CCFULL is also shown. The CN excitation energy (E^*) is shown on the top of X-axis.

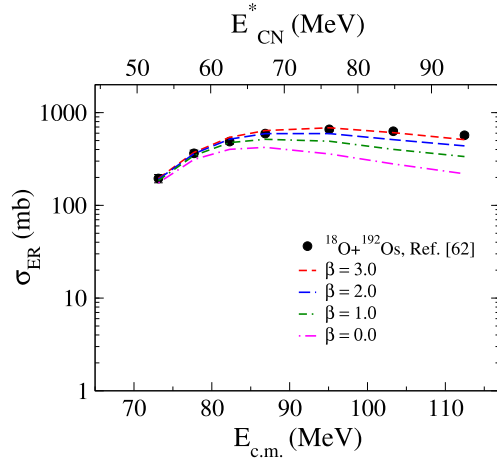


Figure 7. Experimental ER cross sections for $^{18}\text{O}+^{192}\text{Os}$ reaction [62] compared with statistical model calculations using different values of β (in unit of 10^{21} s^{-1}). Total fusion cross section calculated using coupled channels code CCFULL is also shown. The CN excitation energy (E^*) is shown on the top of X-axis.

taken into account in the calculations using a Monte Carlo simulation. The evolution of the CN is followed until it undergoes fission or forms an ER. At the end, an ensemble average of the observable quantities are obtained for comparing with experimental results.

The results of statistical model calculations of ER excitation function using Kramers' fission width Γ_K for the $^{18}\text{O}+^{194}\text{Pt}$ reaction forming the CN ^{212}Rn are shown in figure 4 along with the experimental cross sections. We restrict the calculations to beam energies above the Coulomb barrier. This is because the fission cross section is a small fraction of the total fusion

cross section at energies below the Coulomb barrier and the changes in fission widths would not make any appreciable effect on the ER cross sections. It is observed that calculated values with $\beta = 0$ considerably underpredicts the ER cross sections. However, calculations with $\beta = 3 \times 10^{21} \text{ s}^{-1}$ reproduces the experimental ER cross sections reasonably well.

In order to compare the results of statistical model analysis of the present system with other compound nuclei in the same mass region, similar calculations using free energy profile were next performed for the system $^{16}\text{O}+^{194}\text{Pt}$ leading to the CN ^{210}Rn for which experimental ER cross sections along with a statistical model analysis were earlier reported [36]. In [36], statistical model calculations were performed using potential energy without consideration of shell effects on the fission barrier and, further, constant values for the harmonic oscillator frequencies ω_g and ω_s were assumed which are spin and temperature dependent in the present work. Statistical model results for the ER excitation function for the $^{16}\text{O}+^{194}\text{Pt}$ reaction using Kramers' fission width with shell-corrected fission barrier are shown in figure 5 along with the experimental data. The dissipation strength β required to fit the experimental data lies in the range $(2.0\text{--}3.0) \times 10^{21} \text{ s}^{-1}$ for the above reaction. The experimental values of ER survival probability ($\sigma_{\text{ER}}/\sigma_{\text{fusion}}$) for the $^{16,18}\text{O}+^{194}\text{Pt}$ reactions are plotted in figure 8(a) along with the best-fit statistical model results.

Continuing the statistical model analysis of systems in the same mass region, we next considered the $^{16}\text{O}+^{186}\text{Os}$ and $^{18}\text{O}+^{192}\text{Os}$ systems forming compound nuclei ^{202}Po and ^{210}Po , respectively. The experimental ER and fission cross section data are taken from the literature for these systems [62–64]. Statistical model results for the ER excitation function for the $^{16}\text{O}+^{186}\text{Os}$ and $^{18}\text{O}+^{192}\text{Os}$ reactions using Kramers' fission width with shell-corrected fission barrier are shown in figures 6 and 7, along with the experimental data. The ER survival probabilities extracted using the ER and fission cross sections for the above systems are shown in figure 8(b). The best-fit statistical model results are also shown in figure 8(b). The results indicate that for both Rn and Po isotopes, fission becomes slower with increase of neutron number. Similar observation was also made in earlier works [23, 43].

5. Discussion

The present analysis thus indicates that β values in the range $(1.5\text{--}3) \times 10^{21} \text{ s}^{-1}$ are required to fit the experimental ER cross sections for $^{210,212}\text{Rn}$ and $^{202,210}\text{Po}$ compound nuclei. Two important observations may be made from these results. First, the need for non-zero dissipation coefficients to fit the ER cross section data for the above mentioned systems provides evidence for the dissipative dynamics of hot fused systems in 200 mass region. Similar observations were also made in this mass region via ER cross section [35, 42] and pre-scission neutron multiplicity measurements [51, 65]. In a Langevin dynamical calculation, reasonable agreement with experimental observables was obtained for the compound nuclei $^{206,210}\text{Po}$ [66] where a shape-dependent dissipation with strength varying in the range $(0\text{--}3) \times 10^{21} \text{ s}^{-1}$ [67] is used. The shape-independent β values obtained in the present work are also in the same range.

The second observation concerns the isotopic dependence of the best-fit dissipation strength. Though both ^{212}Rn and ^{210}Po have 126 neutrons, no marked shell closure effect is observed in the dissipation strength. One possible explanation for the above observation is as follows. Most of the compound nuclei in the present study emit a number of neutrons before undergoing fission. Fission can take place for any of the daughter nuclei populated during successive emission of neutrons (or other light particle). Therefore, the total fission cross section is the cumulative effect of fission of a number of daughter nuclei at different excitation

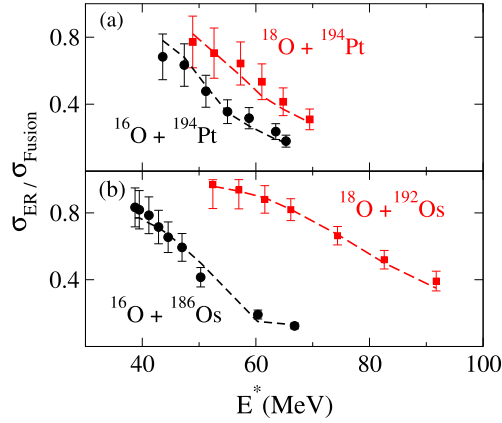


Figure 8. ER survival probabilities for (a) $^{16,18}\text{O}+^{194}\text{Pt}$ and (b) $^{16}\text{O}+^{186}\text{Os}$, $^{18}\text{O}+^{192}\text{Os}$ reactions as a function of CN excitation energy. The best fitted β values required for different systems are: β (all in unit of 10^{21} s^{-1}) = 3.0 for $^{18}\text{O}+^{194}\text{Pt}$, 2 for $^{16}\text{O}+^{194}\text{Pt}$, 3.0 for $^{18}\text{O}+^{192}\text{Os}$ and 1.5 for $^{16}\text{O}+^{186}\text{Os}$.

energies including the initial CN. Consequently, no discernible shell closure effect may survive in the final observables.

It may be remarked here that though the dissipation coefficient represents the damping of collective motion associated with fission and is a bulk property of the nucleus, its strength, derived from fitting experimental data, not only accounts for dissipation but also depends on other inputs to the statistical model which control the fission width. For example, fission width depends on the number of collective fission degrees of freedom [68] though the fission width employed in statistical model calculations, including the present work, usually consider only the elongation degree of freedom. Further, fission width depends sensitively on the height of fission barrier and hence depends on the choice of the conservative force in the fission process. The free energy barrier height is temperature dependent and is smaller than the potential barrier height [58]. Consequently, fission widths with potential energy barrier are smaller than those from free energy barrier. This results in no need for fission hindrance in reproducing experimental ER cross sections when potential fission barrier is used. In fact, a reduction of potential barrier height is required to fit experimental ER data [23, 24]. However, fission hindrance is required for pre-scission neutrons (and other light particles and photons) even with fission widths from potential barrier [65]. This observation suggests that further improvement of fission modelling is necessary. Though the use of free energy fission barrier necessitates a fission hindrance to reproduce ER data, simultaneous analysis of ER cross section and pre-scission neutron multiplicity of various systems using free energy fission barrier is required for a better understanding of the fission process.

6. Summary

We have presented experimental ER and fission cross section data for the $^{18}\text{O}+^{194}\text{Pt}$ reaction forming the CN ^{212}Rn . The normal behaviour of fission fragment angular distributions and angular anisotropy at near barrier regions clearly indicate that the system proceeds through true CN formation and subsequent decay. Statistical model analysis of the ER data employing shell-corrected free energy fission barrier height indicates that a dissipation strength around

$3 \times 10^{21} \text{ s}^{-1}$ is required to reproduce the experimental ER cross sections, particularly at higher CN excitation energies. Statistical model analysis of ER excitation functions of a few other systems in the same CN mass region, namely $^{16}\text{O}+^{194}\text{Pt}$, $^{16}\text{O}+^{186}\text{Os}$, and $^{18}\text{O}+^{192}\text{Os}$ also show that dissipation strengths in the range of $(1.5\text{--}3) \times 10^{21} \text{ s}^{-1}$ give reasonable fit to experimental data. This observation supports the dissipative nature of fission dynamics in heavy ion fusion–fission reactions, especially for heavier systems. No significant dependence of the dissipation strength on CN excitation energy is observed. Further, the dissipation strength does not show any noticeable shell closure effect.

Acknowledgments

The authors are thankful to the accelerator staff of IUAC and BARC-TIFR facilities for providing good quality beams. One of the authors (PVL) acknowledges financial support from IUAC, New Delhi, in the form of a fellowship. BRSB acknowledges the financial support through internal grants from Sultan Qaboos University. SK would like to acknowledge the DAE Raja Ramanna Fellowship.

References

- [1] Oganessian Y T and Utyonkov V K 2015 *Rep. Prog. Phys.* **78** 036301
- [2] Oganessian Y 2007 *J. Phys. G: Nucl. Part. Phys.* **34** R165
- [3] Morita K *et al* 2007 *J. Phys. Soc. Japan* **76** 043201
- [4] Hofmann S and Munzenberg G 2000 *Rev. Mod. Phys.* **72** 733
- [5] Beckerman M 1988 *Rep. Prog. Phys.* **51** 1047
- [6] Dasgupta M, Hinde D J, Rowley N and Stefanini A M 1998 *Annu. Rev. Nucl. Part. Sci.* **48** 401
- [7] Back B B, Esbensen H, Jiang C L and Rehm K E 2014 *Rev. Mod. Phys.* **86** 317
- [8] Back B B, Betts R R, Cassidy K, Glagola B G, Gindler J E, Glendenin L E and Wilkins B D 1983 *Phys. Rev. Lett.* **50** 818
- [9] Toke J *et al* 1985 *Nucl. Phys. A* **440** 327
- [10] du Rietz R, Williams E, Hinde D J, Dasgupta M, Evers M, Lin C J, Luong D H, Simenel C and Wakhle A 2013 *Phys. Rev. C* **88** 054618
- [11] Bjornholm S 1982 *Nucl. Phys. A* **387** 51c
- [12] Lebrun C, Hanappe F, Lecolley J F, Lefebvres F, Ngo C, Peter J and Tamain B 1979 *Nucl. Phys. A* **321** 207
- [13] Ramamurthy V S and Kapoor S S 1985 *Phys. Rev. Lett.* **54** 178
- [14] Berriman A C, Hinde D J, Dasgupta M, Morton C R, Butt R D and Newton J O 2001 *Nature* **413** 144
- [15] Hinde D J, Dasgupta M and Mukherjee A 2002 *Phys. Rev. Lett.* **89** 282701
- [16] Tsang M B, Utsunomiya H, Gelbke C K, Lynch W G, Back B B, Saini S, Baisden P A and McMahan M A 1983 *Phys. Lett. B* **129** 18
- [17] Back B B *et al* 1985 *Phys. Rev. C* **32** 195
- [18] Thomas R G *et al* 2008 *Phys. Rev. C* **77** 034610
- [19] Prasad E *et al* 2010 *Phys. Rev. C* **81** 054608
- [20] Williams E *et al* 2013 *Phys. Rev. C* **88** 034611
- [21] Kowal M, Jachimowicz P and Sobiczewski A 2010 *Phys. Rev. C* **82** 014303
- [22] Vermeulen D, Clerc H G, Sahm C C, Schmidt K H, Keller J G, Munzenberg G and Reisdorf W 1984 *Z. Phys. A* **318** 157
- [23] Sagaidak R N and Andreyev A N 2009 *Phys. Rev. C* **79** 054613
- [24] Varinderjit Singh *et al* 2014 *Phys. Rev. C* **89** 024609
- [25] Itkis M G and Ya Rusanov A 1998 *Phys. Part. Nucl.* **29** 160
- [26] Hilscher D and Rossner H 1992 *Ann. Phys. Fr.* **17** 471
- [27] Hinde D J, Hilscher D, Rossner H, Gebauer B, Lehmann M and Wilpert M 1992 *Phys. Rev. C* **45** 1229

- [28] Newton J O, Hinde D J, Charity R J, Leigh J R, Bokhorst J J M, Chatterjee A, Foote G S and Ogaza S 1988 *Nucl. Phys. A* **483** 126
- [29] Vaz L C, Logan D, Duek E, Alexander J M, Rivet M F, Zisman M S, Kaplan M and Ball J W 1984 *Z. Phys. A* **315** 169
- [30] Schad L, Ho H, Fan G Y, Lindl B, Pfoh A, Wolski R and Wurm J P 1984 *Z. Phys. A* **318** 179
- [31] Dioszegi I, Shaw N P, Mazumdar I, Hatzikoutelis A and Paul P 2000 *Phys. Rev. C* **61** 024613
- [32] Hofman D J, Back B B, Dioszegi I, Montoya C P, Schadmand S, Varma R and Paul P 1994 *Phys. Rev. Lett.* **72** 470
- [33] Thoennessen M, Chakraborty D R, Herman M G, Butsch R and Paul P 1987 *Phys. Rev. Lett.* **59** 2860
- [34] Back B B *et al* 1999 *Phys. Rev. C* **60** 044602
- [35] Shidling P D *et al* 2006 *Phys. Rev. C* **74** 064603
- [36] Prasad E *et al* 2011 *Phys. Rev. C* **84** 064606
- [37] Kailas S and Mahata K 2014 *Pramana* **83** 851
- [38] Madhavan N *et al* 2010 *Pramana* **75** 317
- [39] Jhingan A, Sugathan P, Barua S, Das J J, Varughese T, Madhavan N, Nath S and Madhusudhana Rao P V 2004 *Nucl. Instrum. Methods A* **526** 376
- [40] Subramanian E T *et al* to be published
- [41] Nath S *et al* 2010 *Phys. Rev. C* **81** 064601
- [42] Mohanto G *et al* 2013 *Phys. Rev. C* **88** 034606
- [43] Rohit S *et al* 2015 *Phys. Rev. C* **91** 044621
- [44] Nath S 2009 *Comput. Phys. Commun.* **180** 2392
- [45] Viola V E, Kwiatkowski K and Walker M 1985 *Phys. Rev. C* **31** 1550
- [46] Vandebosch R and Huizenga J R 1973 *Nuclear Fission* (New York: Academic Press)
- [47] Sierk A J 1986 *Phys. Rev. C* **33** 2039
- [48] Gavron A 1980 *Phys. Rev. C* **21** 230
- [49] Hagino K, Rowley N and Kruppa A T 1999 *Comput. Phys. Commun.* **123** 143
- [50] Hagino K and Takigawa N 2012 *Prog. Theor. Phys.* **128** 1061
- [51] Rohit S *et al* 2013 *Phys. Rev. C* **87** 014604
- [52] Prasad E *et al* 2012 *Nucl. Phys. A* **882** 62
- [53] Frobrich P and Gontchar I I 1998 *Phys. Rep.* **292** 131
- [54] Ignatyuk A V, Smirenkin G M and Tishin A 1975 *Sov. J. Nucl. Phys.* **21** 255
- [55] Reisdorf W 1981 *Z. Phys. A* **300** 227
- [56] Kramers H A 1940 *Physica* **7** 284
- [57] Bohr A and Mottelson B R 1975 *Nuclear Structure* vol 2 (London: Benjamin)
- [58] Lestone J P and McCalla S G 2009 *Phys. Rev. C* **79** 044611
- [59] Aritomo Y, Wada T, Ohta M and Abe Y 1999 *Phys. Rev. C* **59** 796
- [60] Bhatt K H, Grange P and Hiller B 1986 *Phys. Rev. C* **33** 954
- [61] Jhilam S 2012 *PhD Thesis* Homi Bhabha National Institute (Unpublished)
- [62] Charity R J, Leigh J R, Bokhorst J J M, Chatterjee A, Foote G S, Hinde D J, Newton J O, Ogaza S and Ward D 1986 *Nucl. Phys. A* **457** 441
- [63] van der Plicht J, Britt H C, Fowler M M, Fraenkel Z, Gavron A, Wilhelmy J B, Plasil F, Awes T C and Young G R 1983 *Phys. Rev. C* **28** 2022
- [64] Rafiei R, Thomas R G, Hinde D J, Dasgupta M, Morton C R, Gasques L R, Brown M L and Rodriguez M D 2008 *Phys. Rev. C* **77** 024606
- [65] Varinderjit Singh *et al* 2013 *Phys. Rev. C* **87** 064601
- [66] Schmitt C, Mazurek K and Nadtochy P N 2014 *Phys. Lett. B* **737** 289
- [67] Gargi Chaudhuri Santanu Pal 2001 *Phys. Rev. C* **63** 064603
- [68] Nadtochy P N, Kelic A and Schmidt K H 2007 *Phys. Rev. C* **75** 064614